Micromotors

DOI: 10.1002/anie.201300913

Self-Propelled Micromotors Driven by the Magnesium–Water Reaction and Their Hemolytic Properties**

*Fangzhi Mou, Chuanrui Chen, Huiru Ma, Yixia Yin, Qingzhi Wu, and Jianguo Guan**

Self-propelled micro- and nanomotors, which are defined as micro- and nanodevices capable of converting chemical energy into autonomous motion,[1] can be used to pick up, transport, and release various cargoes within a liquid medium. They have important potential applications, for example, in environmental remediation,[2] drug delivery,[3] protein and cell separation,[4] and biosensors. Various self-propelled micro- and nanomotors, such as the asymmetrical catalytic nanorods,[5] spherical Janus micromotors,[6] and tubular microengines,[7] have been developed based on the propulsion of bubbles, interfacial tension gradients, self-electrophoresis, and self-diffusiophoresis induced by asymmetrical chemical reactions. However, most of these micro- and nanomotors require H_2O_2, acidic, alkaline, Br_2, or I_2 solutions as the fuel sources, and they are considered to be incompatible with living organisms because of their strong oxidation and corrosion effects.[1c] This seriously hinders the most important practical application of self-propelled micro- and nanomotors in diverse biological systems.

Water, a liquid necessary for life, may be used to generate hydrogen or oxygen bubble thrust for micro- and nanomotors on the basis of the active metal–water reaction and the photocatalytic water-splitting reaction.[8] Nevertheless, the systems designed so far based on the photocatalytic water-splitting reaction cannot efficiently produce sufficient bubbles to power the autonomous motion of micro- and nanomotors, while most violently hydrogen-generating active metals like potassium, calcium, and sodium are too unstable in air even at room temperature to be incorporated in the design of micro- and nanomotors. On the other hand, magnesium (Mg) and aluminum (Al) are stable in ambient atmosphere due to the rapid formation of a compact passivation layer of (hydro)-oxides on the surface and thus these metals cannot be used to reduce water to continuously make hydrogen bubbles.[9] To promote the spontaneous reaction of Al with water to generate hydrogen bubble thrust, Wang and co-workers have utilized a process known as liquid metal embrittlement to remove the Al oxide passivation layer, and have successfully developed water-driven Al-Ga/Ti Janus micromotors.[10] However, the liquid metal Ga and the released Al species from the Al–water reaction are toxic to animals and humans.[11] Therefore, it is still not possible to realize biomedical applications with this alloyed Janus micromotor, though it is able to move efficiently in different biological media.

Metallic Mg is biocompatible and has been used as a biodegradable material in metallic implants in humans.[12] Mg^{2+} ion, as the fourth most abundant ion in the human body and a cofactor for more than 300 enzymes, is essential for the proper functioning of many tissues and organs.[13] Platinum (Pt) is stable and highly biocompatible in biological media.[14] This is the context for our work described herein in which we demonstrate a novel hemocompatible Mg/Pt Janus micromotor driven by the Mg–water reaction. In the rational design of this Mg/Pt Janus micromotor, the $Mg(OH)_2$ passivation layer rapidly formed on the exposed Mg surface is dissolved by an aqueous solution of sodium bicarbonate ($NaHCO_3$).[15] Consequently, the reaction between Mg and water is dramatically promoted to continuously generate directional hydrogen bubble propulsion. Our Mg/Pt Janus micromotor exhibits efficient autonomous motion by harvesting energy from water fuels. Factors influencing the motion performance as well as hemolysis were deciphered. The results here pave a novel green way to facilitate the reaction of water with active metals that have a passivation layer on their surface to powerfully propel micromotors. In contrast with the water-driven Al-Ga/Ti Janus micromotors,[10] the Mg/Pt Janus micromotor is friendly to organism, and holds promise for the important biomedical applications, such as drug delivery and cell separation.

In order to fabricate Mg/Pt Janus micromotors, we treated commercial Mg spheres (Figure S1) with a simple asymmetric modification process, as illustrated in Scheme S1 in the Supporting Information. Figure 1 A and the inset show that the as-obtained the Mg/Pt Janus microspheres have an average size of 20 μm. Portions of the Mg surfaces are exposed, and the Pt layer has a thickness of roughly 100 nm. Figure 1 B indicates that the particles have a spherical morphology with an obvious binary heterostructure, in which the Pt is highly concentrated in the left hemisphere while the Mg is equally distributed over the particle. Figure 1 C,D show the

[*] Dr. F. Mou,[+] C. Chen,[+] Dr. Y. Yin, Prof. Q. Wu, Prof. J. Guan
State Key Laboratory of Advanced Technology for Materials Synthesis and Processing, Wuhan University of Technology
122 Luoshi Road, Wuhan 430070 (P.R. China)
E-mail: guanjg@whut.edu.cn
Prof. H. Ma[+]
Department of Chemistry
Wuhan University of Technology (P.R. China)
[+] These authors contributed equally to this work.

[**] This work was supported by the National Natural Science Foundation of China (51002111), the Natural Science Foundation of Hubei Province (2012FFB05101), the Self-Determined and Innovative Research Funds of SKLWUT and Wuhan University of Technology (2013-PY-3), the Fundamental Research Funds for the Central Universities (WUT: 2013-IV-089), the Top Talents Lead Cultivation Project of Hubei Province, and the Subject Leadership Project of Wuhan City (201150530145).

Supporting information for this article is available on the WWW under http://dx.doi.org/10.1002/anie.201300913.

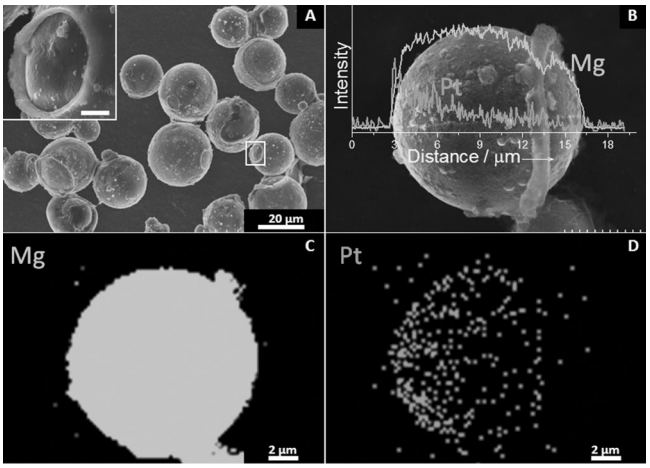

Figure 1. A) SEM images of the as-prepared Mg/Pt Janus spheres; the inset shows the part in the white frame at higher magnification; scale bar: 2 μm. B) The linear EDX analysis of Mg and Pt over a typical Janus microsphere. The mapping EDX images of C) Mg and D) Pt corresponding to the particle shown in (B).

EDX elemental mapping analysis of Mg and Pt, respectively, in the particle imaged in Figure 1B. It further indicates that the surface of the Mg microsphere is partly covered by an asymmetric spherical-cap Pt layer, as expected. It is concluded from Figure 1 that the outer Pt layer compactly covers more than half of the Mg microsphere surface. This facilitates the asymmetrical ejection of H_2 bubbles from the exposed surface of the Mg spheres in water, creating a directional propulsion thrust.

The autonomous movement of the Mg/Pt Janus micromotor was recorded by an optical microscopy. Figure 2 illustrates the self-propulsion of an Mg/Pt Janus micromotor in an aqueous solution containing 0.5 M $NaHCO_3$ and 5% polyvinylpyrrolidone (PVP). Figure 2A–D show the typical time-lapse images taken from Video 1 in the Supporting Information. A long tail of hydrogen bubbles generated on one side of the micromotor is clearly observed, reflecting the rapid spontaneous reaction of Mg with the surrounding water. The hydrogen bubbles of around 10 μm in diameter are ejected at a frequency of about 60 Hz. The as-generated bubbles generate a strong momentum that propels the micromotor forward with a remarkable speed of 75.7 $\mu m\,s^{-1}$, which corresponds to about three body lengths per second. This represents a large driving force of over 190 pN, based on the drag force $F = 6\pi\mu rv$, where r is the radius of the Janus spherical micromotor, v is the speed, and μ is the viscosity of the aqueous medium.[16] Figure 2E shows the tracking trajectory of the Mg/Pt Janus micromotor in water, indicating a spiral motion. The spiral trajectory suggests that the direction of the resultant force from the bubble propulsion and drag resistance changes with time, and its action line is apart from the barycenter or motion direction of the micromotor. This may be ascribed to the asymmetric surface and mass distribution of the Janus micromotor. Similar moving trajectories were previously reported for large rolled-up microengines,[7a] electrosynthesized polyaniline/Pt microtubes,[17] and Pt-nanoparticle-loaded microcapsules.[3] Figure S2 shows the time-lapse images of a typical Mg/Pt Janus micromotor over its whole lifetime, and the average life span of the micromotor is about 77 s, similar to that of Al- and Zn-based micromotors.[7d,10]

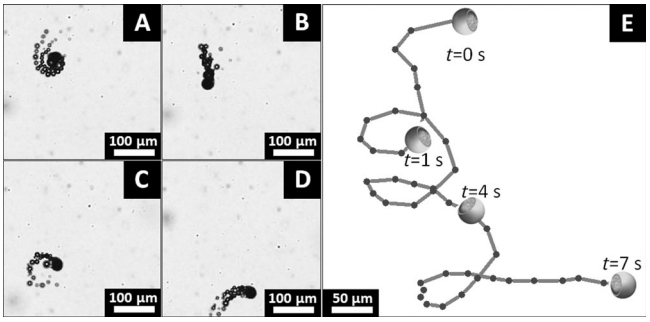

Figure 2. Time-lapse images of a Mg/Pt Janus micromotor driven by the magnesium–water reaction (from Video 1 in the Supporting Information) illustrating the motor propulsion after time intervals of A) 0, B) 1, C) 4, and D) 7 s. E) Motion trajectory of a typical Mg/Pt Janus micromotor suspended in ultrapure water containing 0.5 M $NaHCO_3$ and 5% PVP.

The addition of $NaHCO_3$ plays a crucial role in the self-propulsion of the Janus micromotor. Figure S3 and Video 2 in the Supporting Information indicate that no bubbles are generated when the Mg/Pt Janus microspheres or the Mg microspheres are dispersed in the aqueous medium without $NaHCO_3$. Completely naked Mg microspheres only generate masses of hydrogen bubbles from the entire surface, but no directional movement results when they were dispersed in water containing 0.5 M $NaHCO_3$. This suggests that only with the assistance of $NaHCO_3$ can the Mg microspheres react with water violently to produce abundant hydrogen bubbles. The hydrogen bubbles symmetrically released from the completely naked Mg microspheres do not contribute to the propulsion. In contrast, the Mg/Pt Janus microspheres can autonomously move in the direction opposite to side on which the bubbles are released (Figure 2 and SI Video 1), reflecting the asymmetric bubble generation, which is associated with the blocking effect of the Pt layer upon the Mg–water reaction. From these control experiments it can be seen that the addition of $NaHCO_3$ in water is essential for the continuous Mg–water reaction, and the Janus structure contributes to the asymmetrical generation of hydrogen bubbles and propulsion of the Mg/Pt Janus micromotor.

For the Mg/Pt Janus micromotor, it is water that reacts with Mg to generate hydrogen bubble thrusts and also to form a passivation layer of $Mg(OH)_2$ on the exposed Mg surface, which is rapidly eliminated by $NaHCO_3$ in a sufficiently high concentration (i.e. $[NaHCO_3] = 0.5$ M).[15] As a result, H_2 bubbles are continuously generated from the surface of the exposed Mg to autonomously propel the Janus micromotor. The related chemical reactions are given in Equations (1) and (2).

$$Mg + 2\,H_2O \rightleftharpoons Mg(OH)_2 + H_2 \quad (1)$$

$$Mg(OH)_2 + 2\,HCO_3^- \rightleftharpoons MgCO_3 + CO_3^{2-} + 2\,H_2O \quad (2)$$

In order to confirm this driving mechanism, we have monitored the effect of [$NaHCO_3$] on the amount of hydrogen (Q_{H2}) evolved from an aqueous suspension containing Mg microspheres. Figure S4 shows that Q_{H2} increases with the increasing [$NaHCO_3$]. Figure S5 further indicates that the products collected from the Mg–water reaction in the presence of $NaHCO_3$ are three-dimensional hierarchical nanostructured $MgCO_3{\cdot}3H_2O$ particles. Meanwhile, in our typical experiment the reaction quotient (J) of Equation (2) is calculated to be in the range of 0 and 0.00854, and is always much lower than the equilibrium constant ($K^0 = 17.69$). This suggests that Equation (2) proceeds spontaneously in the forward direction. This confirms that $NaHCO_3$ does not act as a "catalyst", but as a reactant for the dissolution of the $Mg(OH)_2$ passivation layer, as expressed by Equation (2). Since $MgCO_3{\cdot}3H_2O$ has a much higher solubility in water (0.8057 $g\,L^{-1}$) than $Mg(OH)_2$ (9.6×10^{-3} $g\,L^{-1}$) at room temperature,[18] the $Mg(OH)_2$ passivation layer on the exposed Mg surface of the Mg/Pt Janus micromotors is removed by transformation into soluble $MgCO_3$ in water. The fresh Mg surface is then re-exposed to water, causing an intensive and continuous Mg–water reaction. Since the Mg–water reaction on the surface covered by the Pt coating is highly suppressed, the hydrogen bubbles can be released only in a directional way from the exposed Mg surface. As a result, the Mg/Pt Janus micromotors are propelled forward. A schematic diagram of the Mg/Pt Janus micromotors driven by the magnesium–water reaction with the assistance of $NaHCO_3$ is given in Scheme 1.

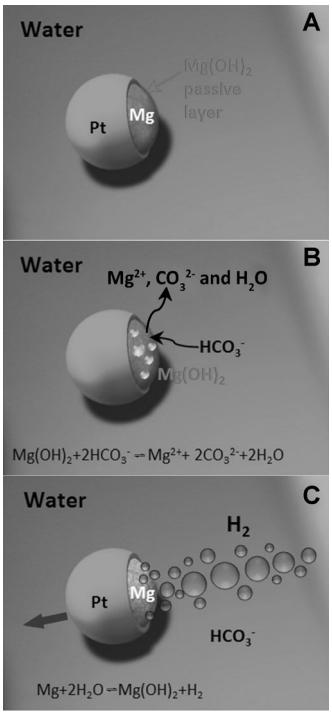

Scheme 1. Schematic diagram of the driving mechanism for the Mg/Pt Janus micromotor: A) the rapid formation of a $Mg(OH)_2$ passivation layer produced by the magnesium–water reaction; B) the $Mg(OH)_2$ passivation layer is removed by reaction with $NaHCO_3$; C) the efficient, directional release of numerous H_2 bubbles from the exposed Mg surface with the assistance of $NaHCO_3$ propels the Mg/Pt Janus micromotor.

The above driving mechanism can be further inferred from the dependence of the autonomous motion of the Mg/Pt Janus micromotors upon [$NaHCO_3$] in water as shown in Video 3 in the Supporting Information. At [$NaHCO_3$] < 0.05 M, no hydrogen bubbles can be observed in the time period of 5 min, indicating that Mg reacts with water in an extremely low rate due to the $Mg(OH)_2$ passivation layer on the Mg surface. At [$NaHCO_3$] $= 0.1$ M, hydrogen bubbles start to be generated on the surface of the micromotor, which, however, shows a rather slow motion as the generated hydrogen bubbles attach to the micromotor and grow slowly over the observing time period. At [$NaHCO_3$] $= 0.5$ M, the Mg/Pt Janus micromotor autonomously moves with a speed of 59–92 $\mu m\,s^{-1}$. Further increasing [$NaHCO_3$] from 0.5 to 1 M has no obvious influence on the speed or the life span of the micromotors, suggesting in this case that the reaction rate of the Mg–water reaction is lower than the rate of the removal of the $Mg(OH)_2$ passivation layer by etching with $NaHCO_3$.[19] The $Mg(OH)_2$ layer newly formed from the reaction of Mg with water can be peeled off in time from the Mg surface by reaction with $NaHCO_3$ to produce water-soluble $MgCO_3$, which diffuses into the water medium with the formation of the hydrogen bubble thrusts and local water flow. Consequently, the hydrogen bubbles are generated at a constant speed by the Mg–water reaction regardless of [$NaHCO_3$], and the Mg/Pt Janus micromotors keep moving with almost constant speed and life span when [$NaHCO_3$] exceeds 0.5 M.

For the as-designed Mg/Pt Janus micromotors, the amount of PVP (W_{PVP}) in water obviously influences on the speed of the autonomous motion. Figure S6 and Video 4 in the Supporting Information show that without PVP in solution, the Mg/Pt Janus micromotor instantly sinks to the bottom and sticks to the glass Petri dish because the viscosity of the aqueous medium is too low to suspend the Mg/Pt Janus micromotor. Meanwhile, although it continuously generates numerous hydrogen bubbles, it does not move because the thrust of the hydrogen bubbles is not strong enough to overcome the friction force between the motor and the bottom surface of the glass Petri dish. When the water fuel contains 5 wt% PVP, the Mg/Pt Janus micromotors can be steadily suspended in it, and they move forward with an average speed of 75.7 $\mu m\,s^{-1}$ under the continuous propulsion of the asymmetrical generation of hydrogen bubbles. Different from the releasing frequency of O_2 bubbles from tube-like micromotors,[20] the Mg/Pt Janus micromotors almost show an independence of the releasing frequencies of hydrogen bubbles on W_{PVP} when it increases from 0 to 5 wt%. When W_{PVP} is further increased to 10 and 20 wt%, the average speed of the Mg/Pt Janus micromotors further decreases to 61.2 and 20.2 $\mu m\,s^{-1}$, respectively. This is because increasing W_{PVP} increases the viscosity of the water fuel, thus enhancing the viscous resistance of the autonomous motion and decreasing the speed of the micromotor.[16b] In addition, increasing W_{PVP} also results in the absorbance of PVP molecules onto the surface of the micromotors, slowing down the reaction rate between Mg and water,[20b] and slightly increasing the life span of the micromotor (Figure S7). This indicates that PVP

mainly acts as a surfactant to facilitate the suspension of the micromotors and their autonomous motion by adjusting the viscosity. It is feasible to replace it with other surfactants, such as benzalkonium chloride and Triton X-100 (see Video 5 in the Supporting Information).

The as-designed Mg/Pt Janus micromotors can operate in biological media and have good hemocompatibility. Figure 3A–C (taken from Video 6 in the Supporting Information) indicates that the Mg/Pt Janus micromotor is efficiently

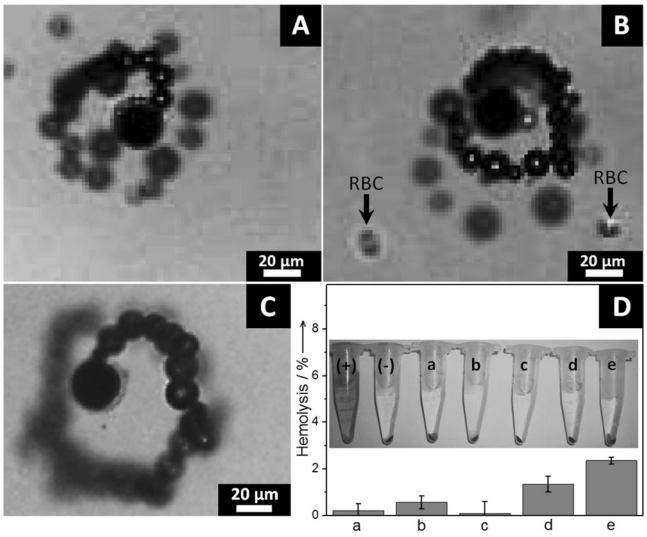

Figure 3. The autonomous movement of the Mg/Pt Janus micromotor dispersed in A) PBS buffer solution, B) a dilute suspension of RBCs in PBS solution containing 0.5 M $NaHCO_3$ and 5 wt% PVP, and C) rabbit serum containing 0.5 M $NaHCO_3$. D) Hemolytic assay for the PBS solution containing a) 0.05 g L^{-1} Mg/Pt Janus micromotors, b) 0.5 M $NaHCO_3$, c) 5 wt% PVP, d) 0.5 M $NaHCO_3$ + 5 wt% PVP, and e) 0.05 g L^{-1} Mg/Pt Janus micromotors + 0.5 M $NaHCO_3$ + 5 wt% PVP. Evaluation scale: highly hemocompatible (< 5% hemolysis); hemocompatible (within 10% hemolysis); non-hemocompatible (> 20% hemolysis). The inset shows the corresponding hemolysis photographs of RBCs. The presence of red hemoglobin in the supernatant indicates damaged RBCs. PBS (−) and deionized water (+) were used as negative and positive controls, respectively.

self-propelled in the phosphate buffer saline (PBS) buffer solution, and in the dilute suspension of red blood cells (RBCs) in PBS containing 0.5 M $NaHCO_3$ and 5 wt% PVP, as well as in the rabbit serum containing 0.5 M $NaHCO_3$, respectively. The speed of the micromotor is about 70 μm s^{-1}. In Figure 3B, the diameter of the H_2 bubbles produced from the Mg/Pt Janus micromotors are similar to that of RBCs, implying that the bubbles and micromotors may have no adverse effects on human body.[21] Figure 3D indicates that the percentages of hemolysis are all within 5% for the Mg/Pt Janus micromotors and the components in its fuel medium (such as $NaHCO_3$, PVP, and $NaHCO_3$ + PVP). In particular, the system containing the Mg/Pt Janus micromotors, 0.5 M $NaHCO_3$, and 5 wt% PVP displays only 2.35% hemolysis. This indicates that the Janus micromotor has a negligible influence on the damage of RBCs and is friendly to organisms. Figure 3D also shows that compared to the samples without 0.5 M $NaHCO_3$ (Figure 3D, a and c), those containing 0.5 M $NaHCO_3$ (Figure 3D, b, d, and e) exhibit a relative higher hemolysis rate. This is mainly attributed to the increased osmotic pressure caused by the addition of 0.5 M $NaHCO_3$, because the hemolysis rate increases with increasing ion concentration in PBS buffer solution (Figure S8). Furthermore, the sample containing the Mg/Pt Janus micromotors, 0.5 M $NaHCO_3$, and 5 wt% PVP has a higher hemolysis rate than that containing only an individual component, suggesting that the Mg^{2+} ions and/or the H_2 bubbles released from the Mg–water reaction also slightly increase the hemolysis of RBCs. Owing to the efficient locomotion and good hemocompatibility of the Mg/Pt Janus micromotors in the biological medium, they hold great promise for practical applications.

In conclusion, we have demonstrated a novel biocompatible Mg/Pt Janus micromotor driven by the Mg–water reaction with the assistance of $NaHCO_3$. The addition of $NaHCO_3$ promotes the Mg–water reaction for the asymmetric hydrogen bubble generation through reacting with the $Mg(OH)_2$ passivation layer on the Mg surfaces to form water-soluble $MgCO_3$. The as-developed Mg/Pt Janus micromotor exhibits efficient autonomous motion in water fuel as well as in biological media, and has important potential biomedical applications, such as drug delivery and cell separation, thanks to its excellent hemocompatibility and harmless reaction products.

Experimental Section

In order to fabricate Mg/Pt Janus micromotors, a simple asymmetric modification process for Mg spheres was performed, as illustrated in Scheme S1. At first, some Mg microspheres (average size 20 μm, Figure S1A) were fully scattered (Scheme S1A) on the surface of a glass slide precoated with PVP film (PVP-glass slide), which was designed to partially cover the bottom surface of the Mg microspheres; the glass slide was prepared by dripping 0.2 mL PVP ethanol solution (2 g L^{-1}) on the glass slide and drying at 60 °C for 10 min. The PVP-glass slide with microspheres was then placed in humid air with a relative humidity of 80% and temperature of 25 °C for 5 s (Scheme S1B). During this process, the Mg spheres were partially immersed in the swollen PVP film by moisture absorption, and the bottom surfaces of the Mg spheres were partially covered and fixed by the PVP film after a drying process at 90 °C for 30 min (Scheme S1C). Then the glass slide was blown with dry high-pressure air to remove the unfixed Mg particles and ensure that the Mg particles remaining on the glass slide are partially embedded in the PVP film. After the exposed surfaces had been coated with a platinum layer by ion sputtering for 240 s under a pressure of 0.6 Pa (Scheme S1D), the PVP-glass slide with Mg/Pt Janus microspheres on the surface (Scheme S1E and Figure S1B) were then immersed in 20 mL acetone and sonicated for 10 s to peel off the Mg/Pt Janus microspheres. The separated Mg/Pt Janus microspheres (Scheme S1F) were isolated by centrifugation, washed with absolute ethanol several times, and then dried in vacuum at 40 °C for 8 h. The pits left on the PVP-glass substrate (Figure S1C) suggest that most of the Mg/Pt Janus microspheres were successfully released from the substrate PVP film by sonication.

Scanning electron microscopy (SEM), and energy-dispersive X-ray (EDX) analyses were obtained using a Hitachi S-4800 field-emission SEM (Japan). The phase purity of the products was examined by XRD using a Rigaku D/Max-RB diffractometer at

a voltage of 40 kV and a current of 200 mA with $Cu_{K\alpha}$ radiation ($\lambda = 1.5406$ Å), in the 2θ range from 10 to 90° at a scanning step of 0.02°.

The autonomous motion of the Mg/Pt Janus micromotor (0.05 g L^{-1}) in water or PBS buffer with 0.5 M $NaHCO_3$ and 5 wt% PVP, as well as in the rabbit serum containing 0.5 M $NaHCO_3$ was observed and recorded with an optical microscope (Olympus BX60), coupled with 10 × objectives, and an Olympus digital camera using the Cell Dimension software. As comparisons, the movement of the Mg/Pt Janus microspheres in water with different concentrations of PVP and $NaHCO_3$, as well as bare Mg microspheres in water containing 0.5 M $NaHCO_3$ and 5% PVP, was also observed and recorded. All videos of the micromotor movement were analyzed using ImageJ and Origin 8.5 software. The control experiments for the Mg–water reaction were carried out by dispersing Mg microspheres (0.2 g) in aqueous $NaHCO_3$ solutions with the concentrations of 0, 0.048, 0.111, 0.333, and 0.5 M, and the evolved hydrogen was detected by a gas chromatograph (7890-II, TECHCOMP, China).

To evaluate the cytotoxicity of the Mg/Pt Janus micromotors, hemolytic assays for the Mg/Pt Janus micromotors and their fuel medium were conducted according to a reported procedure[22] by using heparin-stabilized blood from a healthy New Zealand rabbit.

Received: February 1, 2013
Published online: June 5, 2013

Keywords: hydrogen production · Janus particles · magnesium · micro/nanomotors · water

[1] a) G. A. Ozin, I. Manners, S. Fournier-Bidoz, A. Arsenault, *Adv. Mater.* **2005**, *17*, 3011 – 3018; b) D. A. Wilson, R. J. M. Nolte, J. C. M. van Hest, *Nat. Chem.* **2012**, *4*, 268 – 274; c) J. Wang, W. Gao, *ACS Nano* **2012**, *6*, 5745 – 5751; d) S. Sundararajan, P. E. Lammert, A. W. Zudans, V. H. Crespi, A. Sen, *Nano Lett.* **2008**, *8*, 1271 – 1276; e) S. Sengupta, M. E. Ibele, A. Sen, *Angew. Chem.* **2012**, *124*, 8560 – 8571; *Angew. Chem. Int. Ed.* **2012**, *51*, 8434 – 8445.

[2] M. Guix, J. Orozco, M. García, W. Gao, S. Sattayasamitsathit, A. Merkoçi, A. Escarpa, J. Wang, *ACS Nano* **2012**, *6*, 4445 – 4451.

[3] Y. Wu, Z. Wu, X. Lin, Q. He, J. Li, *ACS Nano* **2012**, *6*, 10910 – 10916.

[4] S. Balasubramanian, D. Kagan, C. M. J. Hu, S. Campuzano, M. J. Lobo-Castanon, N. Lim, D. Y. Kang, M. Zimmerman, L. F. Zhang, J. Wang, *Angew. Chem.* **2011**, *123*, 4247 – 4250; *Angew. Chem. Int. Ed.* **2011**, *50*, 4161 – 4164.

[5] a) W. F. Paxton, K. C. Kistler, C. C. Olmeda, A. Sen, S. K. St. Angelo, Y. Cao, T. E. Mallouk, P. E. Lammert, V. H. Crespi, *J. Am. Chem. Soc.* **2004**, *126*, 13424 – 13431; b) R. Liu, A. Sen, *J. Am. Chem. Soc.* **2011**, *133*, 20064 – 20067.

[6] a) J. R. Howse, R. A. L. Jones, A. J. Ryan, T. Gough, R. Vafabakhsh, R. Golestanian, *Phys. Rev. Lett.* **2007**, *99*, 048102; b) L. Baraban, D. Makarov, R. Streubel, I. Moench, D. Grimm, S. Sanchez, O. G. Schmidt, *ACS Nano* **2012**, *6*, 3383 – 3389; c) W. Gao, M. D'Agostino, V. Garcia-Gradilla, J. Orozco, J. Wang, *Small* **2013**, *9*, 467 – 471.

[7] a) Y. Mei, G. Huang, A. A. Solovev, E. B. Ureña, I. Mönch, F. Ding, T. Reindl, R. K. Y. Fu, P. K. Chu, O. G. Schmidt, *Adv. Mater.* **2008**, *20*, 4085 – 4090; b) K. M. Manesh, M. Cardona, R. Yuan, M. Clark, D. Kagan, S. Balasubramanian, J. Wang, *ACS Nano* **2010**, *4*, 1799 – 1804; c) A. A. Solovev, Y. F. Mei, E. B. Urena, G. S. Huang, O. G. Schmidt, *Small* **2009**, *5*, 1688 – 1692; d) W. Gao, A. Uygun, J. Wang, *J. Am. Chem. Soc.* **2012**, *134*, 897 – 900.

[8] a) M. M. Markowitz, *J. Chem. Educ.* **1963**, *40*, 633; b) A. Kudo, Y. Miseki, *Chem. Soc. Rev.* **2009**, *38*, 253 – 278; c) F. Mou, C. Chen, J. Guan, D.-R. Chen, H. Jing, *Nanoscale* **2013**, *5*, 2055 – 2064; d) L. Li, L. Xu, W. Shi, J. Guan, *Int. J. Hydrogen Energy* **2013**, *38*, 816 – 822; e) L. Xu, J. Guan, W. Shi, *ChemCatChem* **2012**, *4*, 1353 – 1359.

[9] I. A. Taub, W. Roberts, S. LaGambina, K. Kustin, *J. Phys. Chem. A* **2002**, *106*, 8070 – 8078.

[10] W. Gao, A. Pei, J. Wang, *ACS Nano* **2012**, *6*, 8432 – 8438.

[11] a) G. Berthon, *Coord. Chem. Rev.* **1996**, *149*, 241 – 280; b) G. Berthon, *Coord. Chem. Rev.* **2002**, *228*, 319 – 341.

[12] A. L. Di Virgilio, M. Reigosa, M. F. L. de Mele, *J. Biomed. Mater. Res. Part B* **2011**, *99B*, 111 – 119.

[13] I. Slutsky, N. Abumaria, L.-J. Wu, C. Huang, L. Zhang, B. Li, X. Zhao, A. Govindarajan, M.-G. Zhao, M. Zhuo, S. Tonegawa, G. Liu, *Neuron* **2010**, *65*, 165 – 177.

[14] A. Cowley, B. Woodward, *Platinum Met. Rev.* **2011**, *55*, 98 – 107.

[15] a) O. S. Pokrovsky, J. Schott, A. Castillo, *Geochim. Cosmochim. Acta* **2005**, *69*, 905 – 918; b) J. Hövelmann, C. V. Putnis, E. Ruiz-Agudo, H. Austrheim, *Environ. Sci. Technol.* **2012**, *46*, 5253 – 5260; c) L. Wang, T. Shinohara, B.-P. Zhang, *J. Alloys Compd.* **2010**, *496*, 500 – 507.

[16] a) J. G. Gibbs, Y. P. Zhao, *Appl. Phys. Lett.* **2009**, 94; b) D. Bolten, M. Türk, *J. Chem. Eng. Data* **2011**, *56*, 582 – 588.

[17] W. Gao, S. Sattayasamitsathit, J. Orozco, J. Wang, *J. Am. Chem. Soc.* **2011**, *133*, 11862 – 11864.

[18] a) M. Dong, W. Cheng, Z. Li, G. P. Demopoulos, *J. Chem. Eng. Data* **2008**, *53*, 2586 – 2593; b) S. Agarwal, S. R. Al-Abed, D. D. Dionysiou, *Appl. Catal. B* **2009**, *92*, 17 – 22.

[19] J. Hövelmann, C. V. Putnis, E. Ruiz-Agudo, H. Austrheim, *Environ. Sci. Technol.* **2012**, *46*, 5253 – 5260.

[20] a) A. A. Solovev, S. Sanchez, M. Pumera, Y. F. Mei, O. G. Schmidt, *Adv. Funct. Mater.* **2010**, *20*, 2430 – 2435; b) A. A. Solovev, E. J. Smith, C. C. B. Bufon, S. Sanchez, O. G. Schmidt, *Angew. Chem.* **2011**, *123*, 11067 – 11070; *Angew. Chem. Int. Ed.* **2011**, *50*, 10875 – 10878.

[21] S. R. Sirsi, M. A. Borden, *Bubble Sci. Eng. Technol.* **2009**, *1*, 3 – 17.

[22] Y.-S. Lin, C. L. Haynes, *J. Am. Chem. Soc.* **2010**, *132*, 4834 – 4842.

